

Performance of a low-parasitic frequency domain multiplexing architecture

**A.E. Lowitz¹ · P. Barry^{1,2} · A. N. Bender^{1,2} · T.
W. Cecil² · C. L. Chang^{1,2} · R. Divan³ · M. A.
Dobbs⁴ · A. J. Gilbert⁴ · S. E. Kuhlmann² · M.
Lisovenko⁵ · J. Montgomery⁴ · V. Novosad⁵ ·
S. Padin^{1,2} · J. E. Pearson⁵ · G. Wang² · V.
Yefremenko² · J. Zhang²**

the date of receipt and acceptance should be inserted later

Abstract Frequency division multiplexing (FDM) is a readout technique for transition edge sensor-based bolometer arrays used on telescopes including SPT-3G, POLARBEAR-2, and LiteBIRD. Here we present the latest progress and plans for development of a minimal-parasitic FDM architecture. This technology will enable ultra-large focal planes for future instruments such as CMB-S4. Decreased wiring length between the MHz resonators and series SQUID array reduces parasitic impedances which contribute to crosstalk and limit operation of low-resistance bolometers. We have demonstrated improved electrical performance including reduced stray inductance and reduced stray resistance. This will enable operation of low-resistance bolometers and higher multiplexing factors in future arrays. Operating bolometers at lower resistance will decrease the contribution of readout noise to the total NEP by decreasing the required voltage bias. Ongoing work seeks further improvement in circuit parasitics and a laboratory demonstration of this architecture integrated with low-resistance bolometers.

Keywords frequency domain multiplexing, transition edge sensors

1 Introduction

Frequency domain multiplexing (FDM or fMux) is a technique to read out many transition edge sensor (TES) bolometers on a single pair of wires. One LC filter is connected to each bolometer, assigning that bolometer a unique readout frequency and forming an LRC resonator. Signals from all of the LRC resonators are combined, amplified using a cryogenic amplifier (typically a SQUID array), and the individual frequencies for each bolometer are later demodulated in room temperature digital electronics. In the digital frequency domain multiplexing architecture used by SPT-3G (dfMux), 64 bolometers are read out on a single pair of wires⁵. The LRC signal is inductively coupled to a series squid array (SSA) chip

¹Kavli Institute for Cosmological Physics, University of Chicago, Chicago, IL

²High-Energy Physics Division, Argonne National Laboratory, Argonne, IL

³Center for Nanoscale Materials, Argonne National Laboratory, Argonne, IL

⁴Department of Physics, McGill University, Montreal, QC

⁵Materials Sciences Division, Argonne National Laboratory, Argonne, IL

on the 4 K stage. To maximize the effective dynamic range of the SSA, baseband feedback is applied as a nulling signal at the SSA input. This ‘nuller’ is the science signal. Closely-related readout architectures are used by Polarbear-2⁶ and others^{7,8}. This architecture has demonstrated good on-sky performance with SPT-3G^{2,3} with multiplexing factors of up to 68x, but could benefit from improved scalability when applied to future ultra-large focal planes such as those for CMB-S4.

2 Motivation

In the dfMux system, the LC filters which assign a different readout frequency to each bolometer are on the ~ 250 mK stage, near the detectors. A multiplexing unit of bolometers (64 bolometers in the case of SPT-3G) is called a comb. The SQUID chip is on the 4K stage. Wiring between the LC chip and the SQUID chip consists of broadside-coupled NbTi wires encapsulated in Kapton and ultrasonically soldered to the LC circuit board on the 250 mK end and to a breakout circuit board on the 4 K end. The dominant source of crosstalk in the cold portion of the readout is stray impedance in this wiring, (shown in thick, red lines in Fig. 1) which allows the SQUID chip to sit on the 4 K stage, physically distant from the LC filters. Stray impedance in this part of the circuit sets up a voltage divider effect such that when the resistance of one bolometer varies, the ratio of the voltage divider is likewise modulated, resulting in a modulation of the voltage bias supplied to all of the other bolometers⁴. Parasitic resistance in this part of the circuit also contributes to a lower limit on the in-transition resistance of operable bolometers because the parasitic resistance must be small compared to the bolometer resistance to achieve stable bolometer tuning and operation.

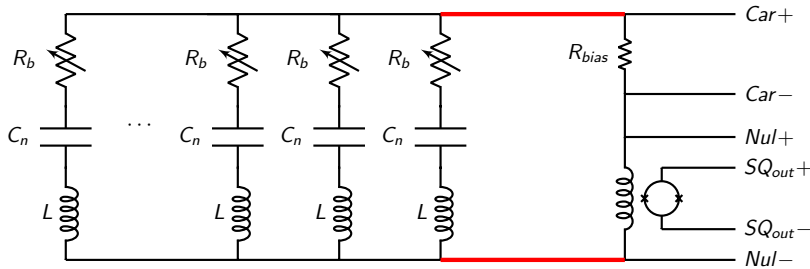


Fig. 1 Schematic showing the cold dfMux circuit. The wiring between the LC chip and the SQUID is indicated by thicker, red lines. This wiring is the dominant source of crosstalk in the cold portion of the dfMux readout, as discussed in section 2. L and C labels indicate the planar superconducting inductors and capacitors of the LC filters. The R label indicated the variable resistance TES bolometer. (Color figure online.)

The primary goal of this work is to develop a modified dfMux (mfMux) architecture which minimizes the parasitic impedance of the wiring between the LC filters and the SQUID. This will substantially reduce crosstalk from the ‘voltage divider effect’ described above. It will also decrease the parasitic resistance in the cold readout, which will enable operation of lower-resistance bolometers. Lower resistance bolometers can be operated with a smaller voltage bias, which allows for a smaller relative contribution of readout noise to the total noise.

3 Design

The design of the modified dfMux hardware to accommodate relocation of the SQUID chip to the 250 mK stage retains as much as possible of the existing dfMux design, which is a mature technology with over two years of successful on-sky demonstration³. By making minimal changes, the mfMux design reaps the benefits of reduced crosstalk, reduced parasitic resistance, and improved scalability, while retaining as much technological maturity as possible. To that end, the mfMux circuit board is identical to the SPT-3G LC board from the input to the LC chip through to the connections to the detector wafer. A small extension was added to the input end of the board to accommodate the SQUID chip. This allows the SQUID chip to be very close to the LC chip, minimizing wiring length between them. Each circuit board houses one LC chip and one SQUID chip on each side. Additionally, the extension to the board is short enough that the mfMux prototype hardware fits in every SPT-3G cryogenic testbed (and in principle, in the telescope itself) as a drop-in replacement for the standard SPT-3G dfMux readout hardware. This enables rapid and straightforward testing of the mfMux architecture alongside SPT-3G hardware for comparison. Refer to Fig. 2 for photographs of the mfMux circuit board design.

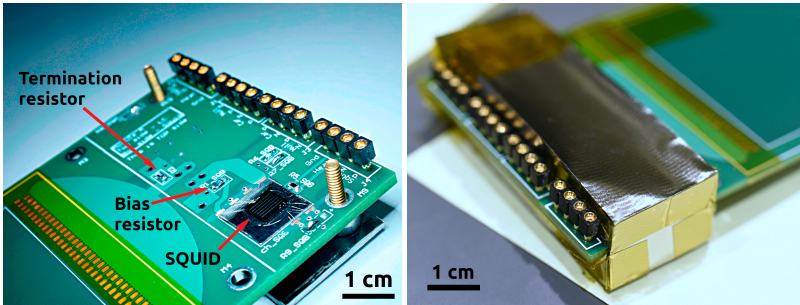


Fig. 2 placeholder photos. I have nicer ones I still need to put labels on. *Left:* Partially-assembled mfMux circuit board showing the SQUID chip, bias resistor, and SIP connectors. *Right:* Fully-assembled mfMux circuit board showing the Metglas cover for the SQUIDs. (Color figure online.)

SQUIDs are sensitive magnetometers and require careful magnetic shielding in order to operate optimally as an amplifier. An aluminum box covered with six layers of Metglas, shown in Fig. 2, covers the mfMux SQUIDs. Comparison testing has shown that the Metglas and aluminum box performs as well as an Ammuneal shield in this application¹. An aluminum cover provides mechanical and magnetic shielding to the LC chips.

A convenient additional benefit of eliminating the long wiring between the LC chip and the SQUID chip is elimination of the need for the custom, labor-intensive, and delicate Kapton-encapsulated broadside-coupled NbTi cabling currently used in the dfMux system to connect from the 4 K stage to the detector stage. Long wiring is still required to reach from the detector stage to the 4 K stage. However, since the long wiring in the mfMux system is between the SQUID output and the warm electronics (instead of between the SQUID and the LC), the impedance of the long wiring does not contribute significantly to crosstalk. Therefore it can be simply replaced with an off-the-shelf, less expensive, more scalable wiring and connectorization solution. The current prototype uses commercially-available NbTi twisted-pair woven ribbon cable, hand-connectorized with SIP socket

connectors. Future revisions may use the same NbTi twisted pair cable with commercially-potted nano-strip connectors for improved scalability.

4 Performance

4.1 SQUID Performance at 250 mK

To date, the mfMux system has been tested primarily using NIST SA-13 SQUID arrays. NIST SA-13s are not necessarily intended for sub-Kelvin operation, however empirically their performance at sub-Kelvin temperatures is comparable to or slightly better than their performance at more typical operating temperatures of 2 - 4 K. Fig. 3 (*Top Left*) shows a comparison plot of the flux bias versus output voltage for the same SA-13 SQUID chip at three temperatures. Performance is very similar at all three temperatures, with a marginal increase in peak-to-peak voltage and transimpedance at lower temperatures. SQUID thermal dissipation is also an important consideration when putting SQUIDs on the same thermal stage as detectors. The thermal dissipation of a SQUID can be estimated as the product of the current bias and the voltage offset at the SQUID output. Fig. 3 (*Top Right*) shows the estimated thermal dissipation for a representative SQUID. Tuned at a typical operating current- and flux- bias, this single SQUID chip (able to operate one comb of bolometers) dissipates about 150 nW of heat onto the detector stage. At this level of thermal dissipation, operating small numbers of SQUIDs on the cold stage in a laboratory testbed works well, but scaling up to the hundreds of SQUIDs required for operation of a large detector array is not feasible with SA-13s using a typical sorption refrigerator. For scalability, either a dilution refrigerator or a lower-thermal dissipation model of SQUID will be required. We plan to measure the actual thermal dissipation of a NIST SA-13 in future work.

4.2 Bolometer Operation and Noise Performance

A previously-published version of the mfMux hardware¹ suffered from a broad in-band resonance. This was related to a wiring error which has since been corrected. With the corrected mfMux hardware, we observe no unexpected resonances. Of a possible 64 bolometers per comb, 58 are operable on the test comb in our current testing configuration. Of the missing six, three are known defects on the detector wafer and three are lithographic defects on the LC chip.

Noise performance of the mfMux prototype overbiased above the TES superconducting transition temperature is comparable to SPT-3G hardware in the same test conditions (see Fig. 3 *Bottom Right*). Of the full comb of 58 bolometers that can be overbiased, we have successfully operated 57 in the TES superconducting transition to an rfrac of $0.2 \times R_{normal}$. For comparison, on the same test wafer during the same cooldown, the standard SPT-3G readout hardware was able to operate at no lower than $0.3 \times R_{normal}$. The improved stability at very low fractional resistances of the mfMux hardware compared to the SPT-3G hardware likely results from the decreased parasitic resistance in the mfMux system, but more investigation is required to develop a detailed understanding of the performance improvements. Fig. 4 shows resistance versus power curves for a representative selection of bolometers being dropped into the TES superconducting transition.

Finally, a side-by-side test of the mfMux and SPT-3G dfMux hardware parasitic resistance demonstrates a factor of two improvement in median parasitic resistance, as shown in

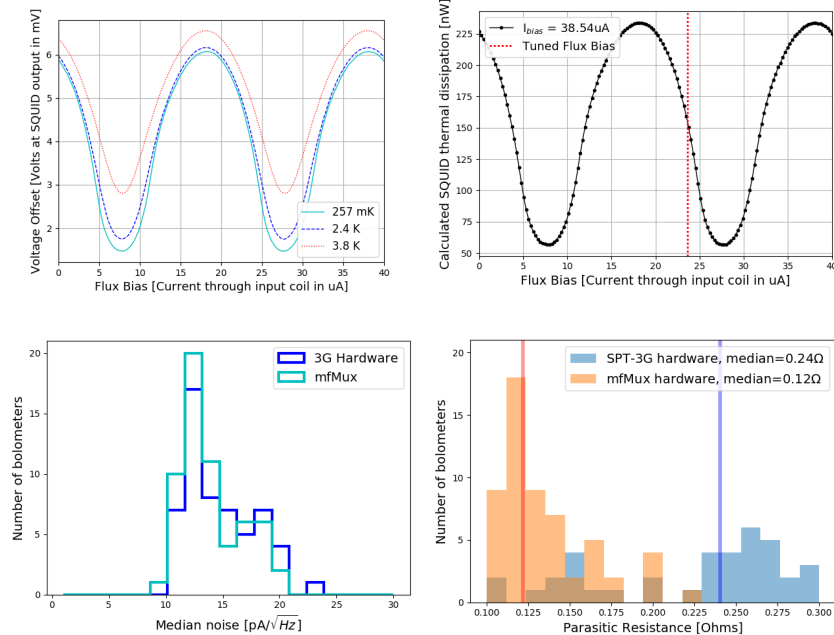


Fig. 3 *Top Left:* Performance of the NIST SA-13 SQUIDS is similar across a range of temperatures. Shown here is the flux bias vs the SQUID voltage offset at three different temperatures for the same SQUID chip at its optimal (maximal peak-to-peak voltage) current bias. At colder temperatures there is a modest increase in peak-to-peak voltage and transimpedance. For this SQUID chip, the transimpedances were $Z=945 \Omega$, $Z=850 \Omega$, and $Z=683 \Omega$ at 257 mK, 2.4 K, and 3.8 K respectively. *Top Right:* The estimated thermal dissipation of a single SQUID at its optimal current bias, calculated from measurements of the flux bias and voltage offset. The vertical red line indicates the tuned flux bias used during typical SQUID operation. *Bottom Left:* The mfMux system has similar low-amplitude warm overbiased noise performance to SPT-3G readout hardware under the same conditions. Shown here are data from a comb of bolometers on SPT-3G hardware and a comb on mfMux hardware, both connected to the same test wafer and measured at nearly the same time in the laboratory. Both combs are biased to a very low amplitude and held above the TES superconducting critical temperature during the measurement. *Bottom Right:* The reduced wiring length between the SQUID chip and LC chip substantially reduces the parasitic resistance in the mfMux system compared to standard dfMux readout hardware. Shown here is the parasitic resistance of one comb of bolometers on mfMux hardware and one comb on SPT-3G hardware, measured at the same time and under the same conditions. The orange and blue vertical lines indicate the medians for the mfMux and SPT-3G hardware respectively. (Color figure online.)

Fig. 3 (*Lower Right*). Lower parasitic resistance will enable operation of lower resistance bolometers, which allows for a reduced relative contribution from readout noise. In future work, we will operate lower-resistance bolometers with the mfMux system.

5 Conclusions and Future Work

In ongoing and future testing of this architecture, focus will be on detailed characterization of the in-transition noise performance and crosstalk performance of bolometers operated with the mfMux hardware in comparison to bolometers operated with the standard dfMux

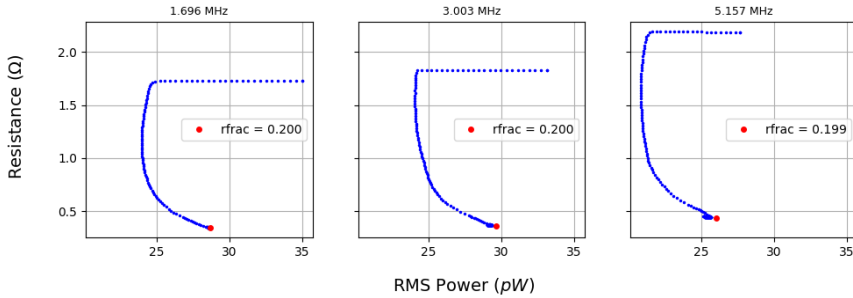


Fig. 4 Operation of a full comb of 57 bolometers down to $rfrac = 0.2 \times R_{normal}$ has been demonstrated with the mfMux prototype. Shown are resistance vs power curves for three representative bolometers as they drop into the superconducting transition. Each bolometer tuning step from overbiased down into the superconducting transition is indicated by a small blue dot and the final tuned point is indicated by a large red dot. The ‘bendback’ feature results from the parasitic resistance, which is significant compared to the in-transition resistance of the bolometers at such low fractional resistances. (Color figure online.)

hardware. Additionally, we plan to make a detailed measurement of the actual thermal dissipation of the NIST SA-13 SQUIDs in this configuration and hope to identify a SQUID model with significantly lower thermal dissipation, which will enable greater scalability without requiring a dilution refrigerator. We also plan to test the mfMux architecture with lower resistance bolometers in the future.

In summary, we have demonstrated operation of a full comb of frequency multiplexed bolometers using the mfMux hardware. Warm overbiased noise performance is comparable to that of SPT-3G hardware under the same conditions, and a past issue with a broad in-band resonance has been resolved. NIST SA-13 SQUIDs perform well overall at sub-Kelvin temperatures, however to enable greater scalability without requiring a dilution refrigerator, SQUIDs with lower thermal dissipation will be required. Broadly, the mfMux architecture shows promise as a more scalable alternative to the standard dfMux system, but more detailed characterization and laboratory testing is required to fully mature this technology.

Acknowledgements Work at the University of Chicago is supported by the National Science Foundation through grant PLR-1248097. Work at Argonne National Lab is supported by UChicago Argonne LLC, Operator of Argonne National Laboratory (Argonne). Argonne, a U.S. Department of Energy Office of Science Laboratory, is operated under contract no. DE-AC02-06CH11357. The McGill authors acknowledge funding from the Natural Sciences and Engineering Research Council of Canada, Canadian Institute for Advanced Research, and the Fonds de recherche du Quebec Nature et technologies.

References

1. A.E. Lowitz, A.N. Bender, M.A. Dobbs, and A.J. Gilbert, *Proc. SPIE, Millimeter, Submillimeter, and Far-Infrared Detectors and Instrumentation for Astronomy IX*. **10708**, 107081D, (2018)
2. A.N. Bender, et al. *Proc. SPIE, Millimeter, Submillimeter, and Far-Infrared Detectors and Instrumentation for Astronomy IX*. **10708**, 1070803, (2018)
3. A.N. Bender, et al. *J. Low Temp. Phys.* **This Special Issue** (2019).
4. M.A. Dobbs et al. *Review of Scientific Instruments*. **83.7**, 073113, (2012)

5. A.N. Bender, et al. *Proc. SPIE, Millimeter, Submillimeter, and Far-Infrared Detectors and Instrumentation for Astronomy VII*. **9153**, 91531A, (2014)
6. D. Barron et al. *Proc. SPIE, Millimeter, Submillimeter, and Far-Infrared Detectors and Instrumentation for Astronomy VII*, **9153**, 915335, (2014)
7. T. Matsumura et al. *J. Low Temp. Phys.* **176**(5-6), 733-740 (2014)
8. B. Reichborn-Kjennerud et al. *Proc. SPIE, Millimeter, Submillimeter, and Far-Infrared Detectors and Instrumentation for Astronomy V*. **7741**, 77411C, (2010)